Optical and Polarimetric SAR Data Fusion Terrain Classification Using Probabilistic Feature Fusion

R. Derek West, David A. Yocky, Brian J. Redman, John D. van der Laan, and Dylan Z. Anderson

Abstract—Deciding on an imaging modality for terrain classification can be a challenging problem. For some terrain classes a given sensing modality may discriminate well, but may not have the same performance on other classes that a different sensor may be able to easily separate. The most effective terrain classification will utilize the abilities of multiple sensing modalities. The challenge of utilizing multiple sensing modalities is then determining how to combine the information in a meaningful and useful way.

In this paper, we introduce a framework for effectively combining data from optical and polarimetric synthetic aperture radar sensing modalities. We demonstrate the fusion framework for two vegetation classes and two ground classes and show that fusing data from both imaging modalities has the potential to improve terrain classification from either modality, alone.

Keywords—*Polarimetric SAR (PolSAR), Optical, Data Fusion, Probabilistic Feature Fusion, Terrain Classification*

I. INTRODUCTION

A given remote sensing modality, such as optical imagery, gives two-dimensional spatial information and measurements from a narrow portion of the electromagnetic (EM) spectrum. Furthermore, with multiple acquisitions of a scene over a time interval, temporal information can also be derived. Combining optical imagery with LiDAR data, for example, can give information on the third spatial dimension. Further combination with another imaging modality, such as synthetic aperture radar (SAR), can extend the EM dimension of information [1].

Combining and utilizing information from multiple sensing modalities can give tremendous more ability than working with data from any given sensor alone. However, combining information from multiple sources is not a trivial problem. There are many articles that address multi-source and multi-temporal data fusion for various purposes, such as fusing SAR and optical data to retrieve soil moisture in vegetated areas [2] and to determine urban land cover [3]. Other researchers have also used SAR and optical imagery for land-cover classification utilizing support vector machines (SVMs) [4], [5], genetic algorithms for feature selection combined with SVMs [6], neural networks [5], and dynamic learning neural networks [7].

In this paper, we use the probabilistic feature fusion (PFF) one-class classifier for terrain classification [8]. PFF-based classifiers may require more up-front feature modeling than other classifiers, but they also offer the advantage of being able to trace decisions back to individual features which many other classifiers do not provide.

II. DATA

The data for this research consists of high-resolution optical and PolSAR imagery. The optical images were collected on June 14, 16, and 18, 2016 and the PolSAR images were collected on March 17, 2016. Figure 1(a) illustrates a pseudo-colored PolSAR image of the scene and figure 1(b) illustrates the optical image of the scene.

A. Optical

The optical images were collected with a commercially available digital single-lens reflex (DSLR) camera with a Bayer RGB filter. The camera was flown on-board an unmanned aerial system (UAS). Sixteen ground control points were setup in the peripheral extremities of the scene to enable geo-referencing the optical images. An automatic white balance adjustment was applied to the optical images. The pixel size of the optical imagery is 0.025 m.

A natural pixel-wise feature vector can be extracted from the R, G, and B (RGB) color channels; however, the color channels tend to be highly correlated for the terrain categories considered. The RGB data were transformed into the CIE 1976 Lab color space and then used to define the optical feature vector,

$$\mathbf{v}_{Opt} = \begin{bmatrix} L & a & b \end{bmatrix}^T. \tag{1}$$

B. Polarimetric SAR

The PolSAR data were collected with the Sandia National Laboratories-developed Facility for Advanced RF and Algorithm Development (FARAD) X-band radar flown on a DHC-6 airplane. The SAR sensor was in videoSAR mode, which continuously collects phase histories around a circular trajectory about the scene center, and collected multiple passes (circular trajectories) of the scene. The stand-off range of the radar to the scene center was nominally 3460 m with a grazing angle of $38°$.

Calibrated polarimetric image sets were formed every $5°$ around the circular trajectories at 0.2032 m range and azimuth resolution. The image sets between two different passes were then co-registered in order to form coherence change detection (CCD) maps [9]. The PolSAR image sets were then processed through the G4U [10] and $H/A/\alpha$ [11] polarimetric decompositions to produce maps of each of the respective parameter sets from the decompositions. The total power (span) maps were also formed from the PolSAR image sets. Finally, the derived parameter maps were multi-looked across $20°$ arcs of the circular trajectory in order to reduce speckle and improve parameter estimates.

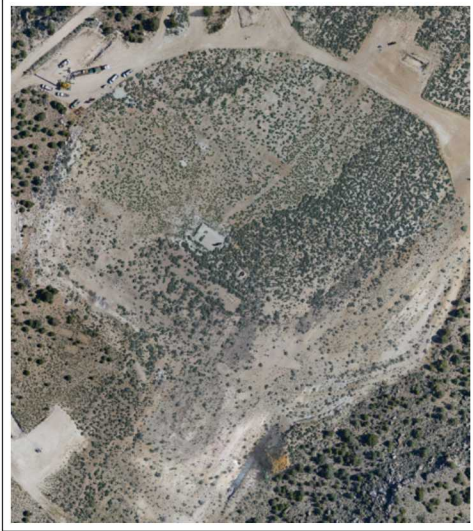A feature vector can be extracted from the multi-looked parameter maps. The feature vector contains the following

elements,

$$\mathbf{v}_{SAR} = [H\ \alpha\ P_s\ P_d\ P_v\ P_c\ Span\ \gamma]^T ,\qquad (2)$$

where $\{H,\ \alpha\}$ are $H/A/\alpha$ decomposition parameters (note the A parameter is not used), $\{P_s,\ P_d,\ P_v,\ P_c\}$ are G4U decomposition parameters, $Span$ is the total power parameter, and γ is the coherence parameter.
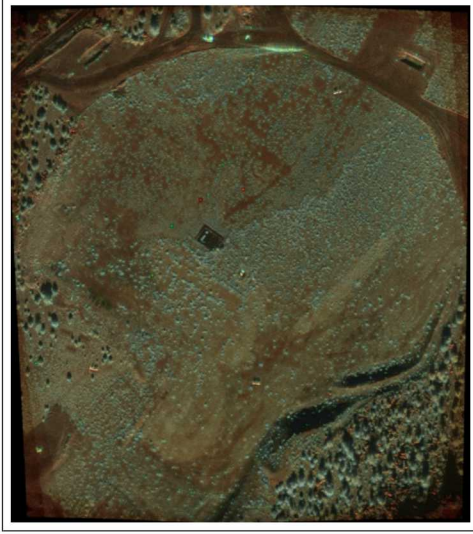
(a)

(b)

Fig. 1. Illustration of the imaged scene from (a) a pseudo-colored, multi-looked PolSAR image, and (b) the optical image.

C. Optical/PolSAR Image Co-Registration

In order to perform data fusion terrain classification, the feature vectors from both the optical and PolSAR data must be co-aligned. The multi-looked PolSAR parameter maps were geo-rectified, the optical images were re-sampled to match the same pixel spacing as the PolSAR parameter maps, and then a manual warping was done to achieve co-aligned pixels. After co-aligning the images sets, the feature vectors from the different imaging modalities can be combined as,

$$\mathbf{v} = \left[\begin{array}{c} \mathbf{v}_{SAR} \\ \mathbf{v}_{Opt} \end{array} \right].\qquad (3)$$

There are unique geometric differences between the two imaging modalities, such as layover in SAR imaging, that have not been compensated. The terrain classes considered here contain classes where geometric differences are negligible.

III. DATA FUSION

In this section, we describe our data fusion terrain classification method. The steps that will be covered include: first, selecting training data for the terrain classes from a joint segmentation of the PolSAR and optical images; second, selecting discriminating features from the combined feature vector for each class; third, modeling the selected features with probabilistic feature fusion.

We selected two vegetation classes, VEG1 and VEG2, and two ground classes, GRD1 and GRD2, to demonstrate the proposed method. Figure 2 illustrates examples of the training data selected from these classes.
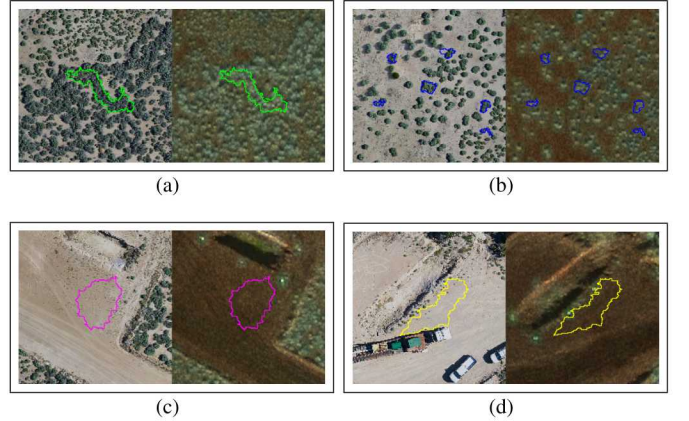

(a)

(b)

(c)

(d)

Fig. 2. Illustration of the terrain classes: (a) VEG1, (b) VEG2, (c) GRD1, and (d) GRD2. On the left is the optical data and on the right is the color-composite PolSAR data. The outlines illustrate examples of selected training data.

A. Selecting Training Data

The selection of training data from heterogeneous data types must be done with care. It may be that the terrain from one imaging modality looks homogeneous, but heterogeneous in the other, due to the measured reflectance or back-scatter. To help ensure training data is consistent for each terrain class, the optical and PolSAR images can be combined. We generated color-composite images of the PolSAR images and used the 'imfuse' command in Matlab to combine the green channel from the optical images and color-composite PolSAR images. We used the combined images along with the PolSAR and optical images to select training and test data.

A superpixel segmentation is then performed on the fused image using the simple linear iterative clustering (SLIC) algorithm [12]. Each superpixel contains relatively homogenous regions of nominally 40 pixels. The training data were selected by selecting superpixels; however, the terrain classification is performed on the pixel data within the superpixels.

B. Feature Selection

The combined feature vector has eleven elements; however, depending on the terrain class, not every element is a useful feature. Plotting pair-wise scatterplots of the feature vector training data allows a way to visualize which feature vector elements discriminate between terrain classes. Figure 3 illustrates a scatterplot of the P_v and b feature vector training data for four terrain classes. In the figure, it is clear that the P_v parameter helps to separate the classes that the b parameter could not do alone, and vice versa.
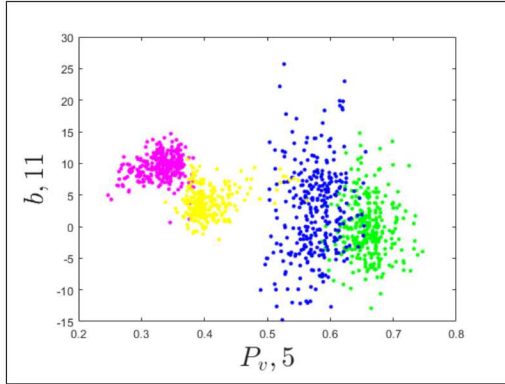

Fig. 3. Illustration of a scatterplot from the P_v and b feature vector superpixel training data for two vegetation classes (green and blue) and two ground classes (yellow and magenta).

C. PFF Classifier

Probabilistic feature fusion (PFF) is a Frequentist framework for one-class classification. The PFF framework allows for defining and selecting discriminating features, each of which are individually modeled. For the data in this paper, each feature in the PFF framework consists of the absolute distance computed from the mean of the selected features from the pair-wise scatterplot training data for each terrain class. Gamma probability distributions fit the metric data well and were used to model the feature data. For the features of a given terrain class, the PFF framework fuses the p-values generated from the gamma distributions to give a final fused p-value. The fused p-value gives a measure of consistency with the training data for each terrain class.

The feature vector elements for the four terrain classes, determined from the scatterplot data, are summarized in table I. Note that the Fused VEG1 and VEG2 PFF models only have PolSAR feature vector elements; however, the GRD1 and GRD2 features include feature vector elements from both imaging modalities. For the VEG1 and VEG2 classes, the

scatterplot data from the optical imagery are highly overlapped, whereas the scatterplot data from both imaging modalities showed separability for the GRD1 and GRD2 classes.

TABLE I.   SELECTED FEATURE VECTORS FOR EACH TERRAIN CLASS AND FOR EACH DATA SET.

	VEG1	VEG2	GRD1	GRD2
RGB	L,a,b	L,a,b	L,a,b	L,a,b
SAR	H,P_d,P_v,P_c	H,P_d,P_v,P_c	H,P_v,γ	H,P_v,γ
Fused	H,P_d,P_v,P_c	H,P_d,P_v,P_c	H,P_v,γ,L,b	H,P_v,γ,L,b

The training data were used to compute the mean for each of the selected features for the absolute distance metric and then gamma distributions were fit to each set of metric data. Figure 4 illustrates the fused p-value output of the four selected features for the VEG1 class for both in-class and out-of-class data.
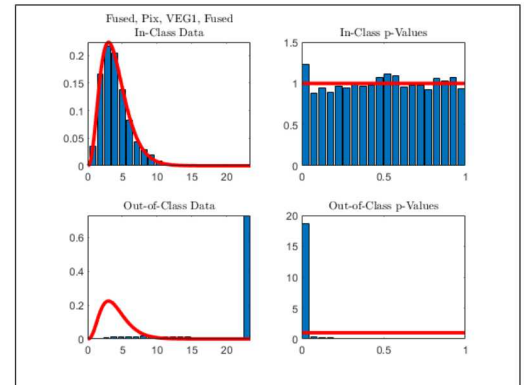

Fig. 4. Illustration of the fusion of selected features for PFF. The upper-left plot illustrates the theoretical probability distribution fit to the fused in-class training data; the upper-right plot illustrates the in-class p-value distribution, which is ideally uniform; the lower-left plot shows that the out-of-class data is very separate from the theoretical in-class distribution; and the lower-right plot shows that the out-of-class samples have low p-values.

IV. RESULTS

To illustrate the proposed heterogeneous terrain classification algorithm, we selected training data for two vegetation classes and two ground class in the training imagery and trained the PFF classifiers for each class. We then applied the PFF classifiers to validation data, selected from the same imagery set as the training data, to determine the performance of the data fusion compared to each imaging modality separately.

Figure 5 illustrates the receiver operating characteristic (ROC) curves of the terrain classifier models from the different imaging modalities and the fusion of them on the validation data. As can be seen from the figure, the fused and the PolSAR data have equivalent performance on the vegetation classes, which is to be expected since the vegetation classes are formed from the same feature vector elements in both cases. The fused ground classes, however, incorporate features from both the optical and the PolSAR data and can be seen to have superior performance compared to either data set alone for the most meaningful regions of the ROC curves.
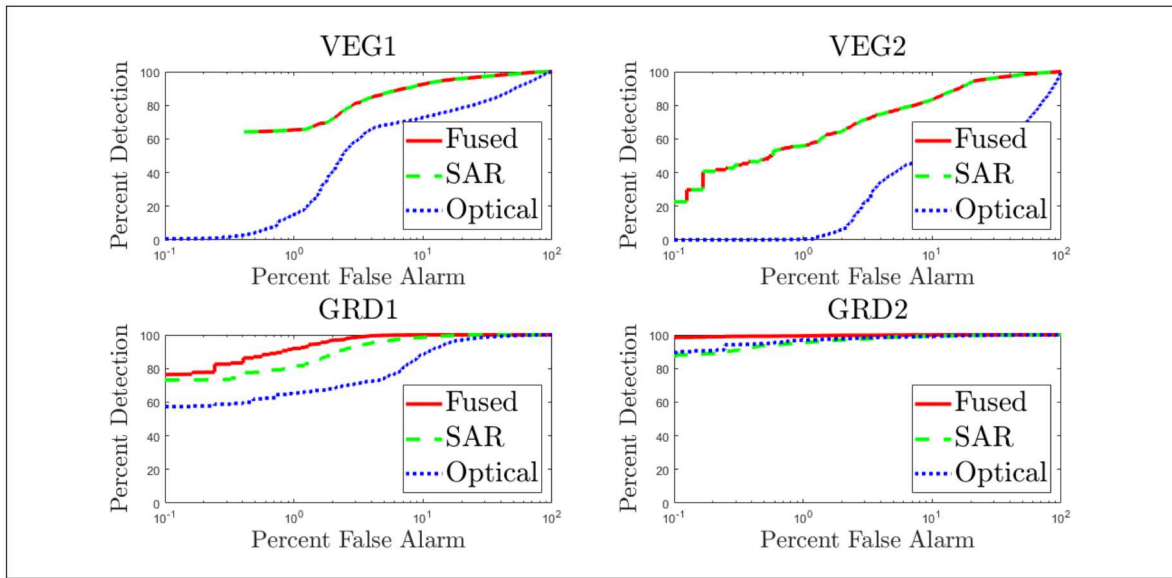
Fig. 5. Illustration of the ROC curves for each terrain PFF model from the optical, PolSAR, and fused data. The fused data can be seen to have equal or superior performance compared to the performance of the data from each separate imaging modality over the meaningful regions of the ROC curve.

V. CONCLUSION

In this paper we introduced and successfully demonstrated an optical and PolSAR data fusion framework for terrain classification using the PFF one-class classifiers. The ROC curves illustrate that adding optical data to the PolSAR data increases the performance of both of the ground terrain classes.

VI. ACKNOWLEDGMENTS

REFERENCES

[1] P. Ghamisi, B. Rasti, N. Yokoya, Q. Wang, B. Hofle, L. Bruzzone, F. Bovolo, M. Chi, K. Anders, R. Gloaguen, P. M. Atkinson, and J. A. Benediktsson, "Multisource and multitemporal data fusion in remote sensing: A comprehensive review of the state of the art," *IEEE Geoscience and Remote Sensing Magazine*, vol. 7, no. 1, pp. 6–39, March 2019.

[2] R. Prakash, D. Singh, and N. P. Pathak, "A fusion approach to retrieve soil moisture with SAR and optical data," *IEEE Journal of Selected Topics in Applied Earth Observations and Remote Sensing*, vol. 5, no. 1, pp. 196–206, Feb 2012.

[3] D. Amarsaikhan, H. Blotevogel, J. van Genderen, M. Ganzorig, R. Gantuya, and B. Nergui, "Fusing high-resolution SAR and optical imagery for improved urban land cover study and classification," *International Journal of Image and Data Fusion*, vol. 1, no. 1, pp. 83–97, 2010.

[4] L. Zhang, B. Zou, J. Zhang, and Y. Zhang, "Classification of polarimetric SAR image based on support vector machine using multiple-component scattering model and texture features," *EURASIP Journal on Advances in Signal Processing*, December 2010.

[5] R. P. H. M. Schoenmakers and L. G. Vuurpijl, "Segmentation and classification of combined optical and radar imagery," in *1995 International Geoscience and Remote Sensing Symposium, IGARSS '95. Quantitative Remote Sensing for Science and Applications*, vol. 3, July 1995, pp. 2151–2153 vol.3.

[6] C. Sukawattanavijit, J. Chen, and H. Zhang, "GA-SVM algorithm for improving land-cover classification using SAR and optical remote sensing data," *IEEE Geoscience and Remote Sensing Letters*, vol. 14, no. 3, pp. 284–288, March 2017.

[7] Y.-C. Tzeng and K.-S. Chen, "Image fusion of synthetic aperture radar and optical data for terrain classification with a variance reduction technique," *Optical Engineering*, vol. 44, no. 10, pp. 1 – 8, 2005. [Online]. Available: https://doi.org/10.1117/1.2113107

[8] K. M. Simonson, R. D. West, R. L. Hansen, T. E. LaBruyere, and M. H. Van Benthem, "A statistical approach to combining multisource information in one-class classifiers," *Statistical Analysis and Data Mining: The ASA Data Science Journal*, vol. 10, no. 4, pp. 199–210, 2017. [Online]. Available: http://dx.doi.org/10.1002/sam.11342

[9] C. V. Jakowatz, Jr., D. E. Wahl, P. E. Eichel, D. C. Ghiglia, and P. A. Thompson, *Spotlight-mode Synthetic Aperture Radar: A Signal Processing Approach*. Springer, 1996.

[10] G. Singh, Y. Yamaguchi, and S. E. Park, "General four-component scattering power decomposition with unitary transformation of coherency matrix," *IEEE Transactions on Geoscience and Remote Sensing*, vol. 51, no. 5, pp. 3014–3022, May 2013.

[11] S. R. Cloude and E. Pottier, "A review of target decomposition theorems in radar polarimetry," *IEEE Transactions on Geoscience and Remote Sensing*, vol. 34, no. 2, pp. 498–518, Mar 1996.

[12] R. Achanta, A. Shaji, K. Smith, A. Lucchi, P. Fua, and S. Süsstrunk, "SLIC superpixels compared to state-of-the-art superpixel methods," *IEEE Transactions on Pattern Analysis and Machine Intelligence*, vol. 34, no. 11, pp. 2274–2282, Nov 2012.